Journal of Environmental Management 346 (2023) 118976

Contents lists available at ScienceDirect

Journal of Environmental Management

journal homepage: www.elsevier.com/locate/jenvman

Research article

Facile and innovative application of surfactant-modified-zeolite from Austrian fly ash for glyphosate removal from water solution

Sarah Haghjoo [a,b,c], Christian L. Lengauer [a,*], Hossein Kazemian [b,c,d,**], Mahmoud Roushani [e]

[a] Universität Wien, Institut für Mineralogie und Kristallographie, Geozentrum (UZA II), Raum 2.B3.48, 1090 Wien, Josef-Holaubek-Platz 2, Austria
[b] Materials Technology & Environmental Research (MATTER) lab, University of Northern British Columbia, Prince George, BC, Canada
[c] Northern Analytical Lab Services (Northern BC's Environmental and Climate Solutions Innovation Hub), University of Northern British Columbia, Prince George, BC, Canada
[d] Environmental Sciences Program, Faculty of Environment, University of Northern British Columbia, Prince George, British Columbia, V2N4Z9, Canada
[e] Department of Chemistry, Faculty of Sciences, Ilam University, Ilam, P. O. BOX. 69315-516, Iran

ARTICLE INFO

Handling Editor: Raf Dewil

Keywords:
Glyphosate
Surfactant-modified-zeolite
Modeling
Adsorption
Leaching

ABSTRACT

This study highlights a pioneering approach in the development of an efficient, affordable, and economically feasible adsorbent specifically tailored for the removal of glyphosate (Gly) from contaminated water. To accomplish this objective, a low-cost and pure NaA Zeolite (NaAZ) was synthesized with 93% crystallinity from Austrian fly ash (AFA) as a precursor for the first-time. Taguchi design was employed to optimize critical parameters such as the SiO_2/Al_2O_3 ratio, alkalinity concentration, time, and temperature. The cation exchange capacity (CEC) and external cation exchange capacity (ECEC) are determined as critical factors for the modification process. Subsequently, the pure NaAZ was modified with hexadecyl trimethyl ammonium chloride (HDTMAC), a cationic surfactant. The utilization of surfactant-modified zeolite (SMZ) for Gly removal demonstrates its innovative application in this field, highlighting its enhanced adsorption capacity and optimized surface properties. The AFA, NaAZ, and SMZ were characterized using analytical techniques including XRD, XRF, FTIR-ATR, SEM, TGA, BET, CHNSO analyzer and ICP-OES. The adsorbent exhibited effective Gly removal through its pH-dependent charge properties (pH 2–10), with an optimized pH 6 facilitating a significant electrostatic interaction between the adsorbent and Gly. SMZ demonstrated remarkable adsorption capacity and removal efficacy, surpassing most reported adsorbents with values of 769.23 mg/g and 98.92% respectively. Our study demonstrates the significant advantage of the SMZ, with a low leaching concentration of only 6 ppm after 60 days, ensuring environmental safety, long-term stability, and public health considerations. The kinetics of the adsorption process was well described by the pseudo-second order and the Freundlich isotherm. Pore diffusion and H-bonding were postulated to be involved in physisorption, whereas electrophilic interactions led to chemisorption type of adsorption. Consequently, SMZ provides a practical significance, broad applicability and promising solution for Gly removal, facilitating sustainable water treatment.

[1] https://www.weforum.org/agenda/2021/08/4-key-steps-decommissioning-coal-fired-power-plants/
[2] https://cleanwater.org/whats-your-water
[3] https://hub.jhu.edu/at-work/2021/10/13/why-you-should-drink-a-glass-of-water/
[5] https://www.chemdraw.co.ac/

1. Introduction

Agriculture, heavily reliant on the use of pesticides and herbicides, plays a pivotal role in global food production, while also raising significant environmental and health considerations (Carneiro et al., 2015). Gly, a non-selective and broad-spectrum herbicide, is extensively used in various commercial products like Roundup to effectively

* Corresponding author. Department of Mineralogy and Crystallography, University of Vienna, UZA-2, Austria.
** Corresponding author. Northern Analytical Laboratory Services, Chemistry Department, Faculty of Science and Engineering, University of Northern British Columbia, Office: #4-257, Canada.
E-mail addresses: christian.lengauer@univie.ac.at (C.L. Lengauer), hossein.kazemian@unbc.ca (H. Kazemian).

https://doi.org/10.1016/j.jenvman.2023.118976
Received 23 June 2023; Received in revised form 28 August 2023; Accepted 9 September 2023
Available online 20 September 2023

eliminate long grasses and broadleaf weeds from major grain crops such as corn, soybean, wheat, and more (Tao et al., 2022; Wang et al., 2024). With its high water solubility (~12 g/L), the chemical demonstrates remarkable mobility, posing concerns for potential leaching and runoff, and thereby impacting surface and groundwater quality (Arroyave et al., 2016; Liang et al., 2020). Therefore, exposure to this type of herbicide has been correlated with a spectrum of detrimental effects, including cardiovascular and respiratory disorders, ocular and dermal inflammation, potential endocrine disruption, and possible pregnancy complications (Myers et al., 2016; Xie et al., 2023). As a result, it is crucial to emphasize the removal of Gly from polluted aqueous systems to mitigate its adverse impacts. Adsorption stands out as a significant and effective approach for the remediation of such pollution, owing to its notable attributes of environmental friendliness, versatility, ease of design, and cost-effectiveness (Mayakaduwa et al., 2016; Li et al., 2021). There are distinctive sorts of adsorbents used for the removal of Gly, such as molecularly imprinted polymers (Do et al., 2015), metal-organic frameworks (Pankajakshan et al., 2018), soils (Graziano et al., 2023), clays (Nargis et al., 2022), biochar (Cederlund et al., 2017) and zeolites (Sittiwong et al., 2022).

Zeolites are the most effective adsorbents among these other varieties due to their porous structure, large specific surface area, high cation exchange capabilities, and inexpensive cost. Zeolites could be synthesized from solid waste material such as Coal fly ash (CFA) produced from coal combustion of coal-fired power plants. Due to the prevalence of amorphous aluminosilicate in CFA, it is a highly potential source for synthesizing various types of green zeolites, such as FAU, LTA, and GIS. NaA (LTA) zeolite was chosen for synthesis in this study due to its exceptional physicochemical properties, including non-toxicity, high porosity, excellent thermal stability, regular internal tunnels, and high cation exchange capacity. These properties make NaA zeolite widely applicable in gas and liquid purification, wastewater treatment. Considering the vast quantities of CFA manufactured (more than 750 million tons per year) (Asl et al., 2018) and the known association with significant environmental and health concerns, such as lung cancer, it is imperative that research be conducted on the managing of CFA.

Therefore, many investigations have been performed on synthesizing zeolitized CFA, its characterization, and its application (Wang et al., 2003; Liu et al., 2013; Attari et al., 2017). However, their inherent hydrophilic nature and negative surface charge can limit the effectiveness of zeolites in adsorbing ionic contaminants. To enhance their hydrophobicity, adsorption capacity, and introduce a positive surface charge, zeolites are often modified with cationic surfactants (Andrunik et al., 2023). For this objective, a quaternary amine containing a long-chain cationic surfactant, such as hexadecyl trimethyl ammonium bromide or chloride (HDTMAB/C), has been utilized (Crocker et al., 1995; Li et al., 1998). HDTMAC is not leached in the solution and, hence, is not toxic to wildlife and microorganisms when attached to zeolite (Choi and Shin, 2020). The application of environmentally friendly, inexpensive materials with a high adsorption capacity is critical for expanding sustainable and efficient techniques for Gly removal.

As far as the authors are aware, although the synthesis of zeolite from coal fly ash has been explored in many studies, there is not any investigating the synthesis of zeolite from AFA which composition was more complex and difficult to synthesize the NaAZ. In addition, data on the effect of cationic surfactant on the properties of zeolite as an adsorbent for removal of Gly has not yet been reported in the literature. Therefore, this study not only demonstrated the potential increase in economic value and mitigation of disposal issues through the conversion of AFA to zeolite but also successfully developed a remarkably proficient, cost-efficient, and unique adsorbent for the removal of Gly, along with postulated mechanisms. A design of experiments (DOE) was utilized to ascertain the optimal parameters for both the zeolite synthesis and the batch adsorption of Glyphosate (Gly). The application of DOE aimed to minimize the number of experiments, reduce errors, enhance process reliability and performance, and decrease costs, time, and energy consumption. The capability of adsorbents was determined to assess the leaching of adsorbed-Gly and heavy metals from AFA, NaAZ, and SMZ. The study examines different isotherm and kinetic models to describe Gly adsorption behavior and discusses potential mechanisms on SMZ adsorbent.

2. Materials and methods

2.1. DOE using Taguchi model

The formation parameters, such as SiO_2/Al_2O_3 ratio, alkalinity concentration, time, and temperature, play a crucial role in determining the type of zeolite formed. Therefore, it is important to evaluate the effects of these parameters and conditions on the synthesis efficiency and characteristics of the synthetic zeolite. The optimization of these parameters at three levels for the synthesis of pure NaAZ from AFA was achieved using a Taguchi L_9 orthogonal array (Dargahi et al., 2012) (Table 1S). The analysis of the results was conducted using Minitab software (version 18, Minitab Inc., USA). The yield and crystallinity percentages of the samples were computed by applying Eqs. (1) and (2) (Ruen-ngam et al., 2009; Aldahri et al., 2017), respectively. To ensure reproducibility, all experiments were performed in triplicate.

$$\text{Yield } \% = W_{sample} / W_{FAFA} * 100 \quad (1)$$

$$\text{Crystallinity } \% = \sum \text{relative intensities of NaA} / \sum \text{relative intensities of reference} \times 100 \quad (2)$$

The weight of the synthesized zeolite (W_{sample}) in g and the weight of the fused AFA (W_{FAFA}) in g are used in the yield calculation. The percentage of crystallization is determined by expressing the ratio of the sum of the relative intensities of the NaAZ obtained from AFA to the sum of its relative intensities in the reference.

2.2. Synthesized pure NaAZ under optimized factors

The optimized parameters derived from the Taguchi design were utilized to synthesize pure NaAZ with a high yield and crystallinity percentage, as detailed in the XRD section. In brief, AFA and NaOH powders (98%, Sigma Aldrich, Canada) were thoroughly pulverized at a weight ratio of 1:2. The resulting mixture was fused at 550 °C for 1 h in a furnace. Subsequently, 6 g of the fused AFA was mixed with 60 mL of distilled water. 0.5 M $NaAl_2O_3$ solution (95%, Sigma Aldrich, Canada) was then added to the reaction mixture. The composition gel was aged at ambient temperature for 8 h (h), and then transferred to a Teflon-lined stainless-steel autoclave, where it was subjected to a temperature of 85 °C for a duration of 6 h to facilitate the crystallization of NaAZ. Finally, the sample was washed with water to eliminate any unreacted and water-soluble components, dried at 105 °C for 7 h, resulting in the synthesis of optimized pure NaAZ (Ameh et al., 2017). In the process of determining zeolite's CEC, the methodology involves achieving equilibrium via ammonium (NH^{+4}) ion exchange, and then replacing NH^{+4} ions with sodium (Na^+) ions as outlined by El-Naggar (El-Naggar et al., 2008). The ICP-OES technique is employed to quantify the concentration of exchangeable ions. The experiment was performed in triplicate.

2.3. Preparation of SMZs

The sorption of surfactant on zeolite surfaces is governed by two critical factors: the ECEC (Hailu et al., 2017) of the NaAZ and the critical micelle concentration (CMC) (Wang and Peng, 2010) of the HDTMAC. These parameters intricately influence the adsorption process, dictating the arrangement and configuration of surfactant molecules on the zeolite surface, thereby leading to the formation of various structures, including monolayers and bilayers. The ECEC value of the NaAZ was determined using a method previously established (Haggerty and Bowman, 1994). This method involved saturating the external

exchangeable sites of the NaAZ with sodium chloride and subsequently exchanging them with HDTMAC (Haggerty and Bowman, 1994). Additionally, in colloidal and surface chemistry, CMC is defined as the concentration of surfactants at which micelles start to form, and additional surfactants added to the solution predominantly produce micelles (Wang and Peng, 2010). When the surfactant concentration in the solution is equal to or lower than the CMC (0.92–1.0 mmol/L for HDTMAC) (Ghiaci et al., 2004), the most probable mechanism (electrostatic mechanism) of surfactant adsorption on a solid surface is the formation of a surfactant monolayer. However, when the surfactant concentration exceeds the CMC, a bilayer of surfactant molecules is attached to the external surface, where the outer layer of surfactant molecules is bound by hydrophobic interactions (Chutia et al., 2009). Hence, in order to produce modified SMZs, 5 g of NaAZ was introduced into a 20 mL solution of HDTMAC (98%, obtained from Sigma-Aldrich, Canada) at concentrations of 1, 20, and 50 mmol/L, which are approximately 0.2, 4, and 10 times higher than the ECEC, respectively. The mixture was then stirred for 3 day at room temperature. Afterward, the resulting samples were washed with an excess of deionized water until no foam formed when shaking the supernatant in a 1:10 solid-to-solution ratio. Finally, the samples were dried for 7 h at 105 °C. As a consequence of the experimental procedure, three distinct samples were generated, each labeled as SMZ1, SMZ20, and SMZ50.

2.4. Batch adsorption studies

2.4.1. Identifying highly effective adsorbent

In this study, it is imperative to compare the adsorption capacities of NaAZ and SMZ with different concentration in various pH to identify the most efficient adsorbent for Gly removal. Consequently, two experiments were carried out to address this objective. 1) Optimizing the pH is crucial for this study due to the surface charge of zeolite. To ensure accurate results and prepare for further experiments, NaAZ and SMZ20 were both tested at a concentration of 1.2 g/L across a pH range of 2–10 for a duration of 24 h. Based on the results, which are detailed in section 3.2.1, a pH of 6 was selected as the benchmark for our research experiments. Additionally, the experiment included the parallel investigation of the pH of the point of zero charge (pHpzc) (Noroozi et al., 2018). 2) Other experiments were carried out using 1.2 g/L of NaAZ, SMZ1, SMZ20, and SMZ50 with a 100 mg/L Gly solution at pH 6 in four polypropylene vials. Based on the results of this experiment, SMZ20 has been selected as the optimized adsorbent in this study for the removal of Gly. This choice was based on its superior performance, as discussed in section 3.2.2. It is worth to mention that, the suspensions of all adsorption experiments were agitated at 150 rpm using a rotating shaker, and subsequent centrifugation allowed for analysis of the supernatants using ion-exchange chromatograph-optical emission spectroscopy (IC-OES). To enhance the robustness of the experimental findings, a triplicate approach was employed for all experiments.

2.4.2. Taguchi-optimal factors

The working solution was prepared from a 1000 mg/L Gly (%98, Sigma Aldrich, Austria) stock solution. The working solution concentration was based on environmental water samples, particularly those from Gly manufacturing. High Gly concentrations in natural waterways are improbable (Battaglin et al., 2009; Hu et al., 2011; Mayakaduwa et al., 2016). Adsorption conditions were optimized using a Taguchi experimental L_{16} array. To optimize adsorption capacity and removal efficiency, initial concentration (5–250 mg/L), adsorbent dose (0.1–2 g/L), and contact time (0.5–24 h) were examined. Table 2S lists experimental variables and levels. Each experiment was triplicated to assess uncontrolled factors. The following equations calculated equilibrium adsorption capacity and removal efficiency (Diel et al., 2021a).

$$q_e = [C_0–C_e]\ V/M \quad (3)$$

$$\text{Removal } \% = [C_0–C_e / C_0] * 100 \quad (4)$$

where q_e is the equilibrium adsorption capacity (mg/g); C_0 and C_e are the initial and equilibrium concentrations of Gly (mg/L), respectively; M is the mass of the adsorbent (g), and V is the volume of solution (L).

2.4.3. Isotherm and kinetics of adsorption

Adsorption isotherm tests were conducted using Gly solutions with concentrations ranging from 100 to 500 mg/L, in combination with 1.2 g/L of SMZ20. The tests were carried out for a duration of 2 h at pH 6. For the kinetics experiments, suspensions containing 1.2 g/L of adsorbent and 100 mg/L of adsorbate were vigorously shaken at 150 rpm on a rotating shaker. The contact times ranged from 5 min to 24 h, and the experiments were performed at pH 6.

2.5. Leaching test

2.5.1. Leaching of heavy metals

The DIN 38414 S4 Germany standard leaching test was employed to examine the leached metal concentrations from AFA, NaAZ and SMZ20. In this test, 1:10 triplicate of samples were stirred for 24 h in ultrapure MilliQ water, filtered, and evaluated by ICP-OES (Kazi et al., 2005).

2.5.2. Leaching of Gly from saturated adsorbents

A leaching test was performed to assess NaAZ and SMZ20's capability to prevent Gly from leaching into the solution. To the authors' knowledge, only a few research has explored the effect of time on the leaching of Gly from saturated adsorbent (Diel et al., 2021b; Milojević-Rakić et al., 2022). This experiment combined 1.2 g of saturated adsorbents (NaAZ-Gly and SMZ20-Gly) with 1 L of distilled water. After 1, 15, and 30 days, the samples were filtered and IC-OES quantified Gly leachate in the supernatants.

2.6. Characterization

Semi-quantitative chemical analysis was conducted using X-ray fluorescence (XRF) on a Rigaku ZSX Primus XRF machine equipped with an end window 4 KW RH-anode X-ray tube (Rigaku, Canada) to identify the chemical composition of the AFA. To determine the crystalline phases of AFA, NaAZ, and SMZ20, X-ray diffraction (XRD) analysis was performed using a Rigaku Miniflex 300 with CuKα (K for Kα = 1.54059 Å) over the range of $5° < 2\theta < 70°$ with a step width of 0.02°. Fourier transform infrared spectroscopy-attenuated total reflection (FTIR-ATR, Canada) was utilized to identify the nature of the functional groups involved in the samples, covering the wavelength range of 400–4000 cm^{-1}. Thermogravimetric analysis - derivative thermogravimetric (TGA-DTG, Canada) was carried out using a TGA1-00744 Canada instrument, heating the samples at a rate of 10 °C/min under nitrogen purge from 25 to 600 °C. The specific surface area (SSA), pore volume, and pore size of the samples were determined using a nitrogen adsorption technique based on the Brunauer–Emmet–Teller (BET, Canada) model, employing the N20-25e Nova 2000e instrument. Scanning Electron Microscopic (SEM, Iran) analysis was performed using a MIRA3 instrument (TESCAN, Canada) to examine the morphology and elemental composition of the samples. The HDTMAC concentrations in the samples were determined based on the carbon concentrations measured using a CHNSO analyzer (Costech 4010 CHNSO analyzer). Elemental concentration analysis of different elements in solutions was conducted using Inductively Coupled Plasma-Optical Emission Spectroscopy (ICP-OES) with an Agilent Technologies 7500cx instrument (Canada).

3. Results and discussion

3.1. Characterization

The major chemical constituents of the AFA, NaAZ and SMZ20 are presented in Table 1, analyzed using the XRF technique. The results of XRF indicate that the AFA falls under class F, as the combined content of SiO_2, Al_2O_3, and Fe_2O_3 exceeds 70% (Bukhari et al., 2015). The low loss on ignition (LOI) value indicates a minimal presence of unburned carbon or organic material in the mixture. It is important to mention that there was an elevation in Na_2O content within the NaAZ. This affirms the successful creation of NaAZ (de Aquino et al., 2020). However, Na_2O reduction in SMZ20 sample suggests the loading of HDTMA on NaAZ through a cation exchange mechanism involving quaternary ammonium cations and Na^+ ions. The SiO_2/Al_2O_3 ratio of AFA (2.1) suggests the requirement of an additional aluminum source for the synthesis of NaAZ, as the typical SiO_2/Al_2O_3 ratios for NaAZ range from 1 to 1.2 M ratios. The intended SiO_2/Al_2O_3 ratio of 1.08 for NaAZ and SMZ20 was the objective during the synthesis of NaAZ. The CEC and ECEC values for AFA and NaAZ provided in Table 1. (Zhang et al., 2013). The raised CEC value compare to AFA demonstrated the exceptional purity level of the zeolite product (93%). (El-Naggar et al., 2008).

The Rietveld fit of the XRD recorded on the AFA powder is shown in Fig. 1 (I). The diffraction data indicate the presence of amorphous and crystalline phases in the AFA. The phases have been identified as amorphous aluminosilicate (42%), quartz (SiO_2, 31%), mullite ($3Al_2O_3{\cdot}2SiO_2$, 25%) and hematite (Fe_2O_3, 2%). The existence of a significantly reactive amorphous aluminosilicate glassy phase, evident as a broad peak between 20° and 25° in the 2θ range, promotes the generation and development of zeolite structures (El-Naggar et al., 2008). Through the conversion process, the predominant crystalline phases of aluminosilicates in AFA was converted into zeolitic crystals via an alkali hydrothermal reaction. The aluminosilicates dissolved into the reaction mixture, forming clusters, nucleating, and growing as crystals on the surface of AFA (Bukhari et al., 2015). The alkalinity, SiO_2/Al_2O_3 molar ratio, crystallization temperature, and reaction time were key factors in zeolite synthesis. A Taguchi design with an L_9 orthogonal array was used to investigate their influence on crystallinity and yield percentage. Results are summarized in Table 3S. The results indicate that the SiO_2/Al_2O_3 molar ratio plays a pivotal role in the crystallization of NaAZ. It has been observed that alterations in the SiO_2/Al_2O_3 molar ratio exert a substantial influence on the nucleation and crystallization processes of diverse zeolite frameworks. This phenomenon can be attributed to the fact that zeolite structures are formed through the three-dimensional linkage of SiO_4^{4-} and AlO_4^{5-} tetrahedra with oxygen atoms. Therefore, increasing the SiO_2/Al_2O_3 ratio from 1 to 2.5 tends to promote the formation of zeolites A, X, and P (Yi et al., 2012). The XRD patterns of the samples (Z1-Z9) depicted in Fig. 1 (II) reveal distinct peaks corresponding to the synthesized NaP1, sodalite (SOD), and NaX and NaA phases during the crystallization process. Moreover, higher NaOH concentrations resulted in increased dissolution of Si and Al from the fly ash, thereby accelerating zeolite formation and causing alterations in properties such as crystallization percentage and peak intensities. (Anbia et al., 2015). This is evident from the intensified XRD peak intensities in Z2, Z4, and Z8 (representing NaP1, NaX, and NaA, respectively). Additionally, the hydrothermal temperature significantly affects the nucleation and crystal growth processes. At higher temperature, the rates of crystallization and nucleation are increased. The formation of zeolite is thermodynamically metastable, so the control of reaction temperature is important. Furthermore, the hydrothermal reaction time also have significant effects on the crystalline morphology of synthetic zeolites. Proper hydrothermal time can obtain the zeolites with relatively uniform particle size and crystals (Chaves et al., 2012). The findings of this study offer valuable insights for the treatment of AFA and the development of innovative recycling methods to create valuable green products from waste AFA. Therefore, the optimum conditions to obtain the NaAZ with 93% crystallinity and 89% yield were found to be temperature level (85 °C), $NaAl_2O_3$ (0.5 M) and AFA/NaOH (1:2 wt ratio) and duration (6 h). The optimal conditions were verified through three separate experiments conducted for run 8, and the results consistently showed that the synthetic zeolite achieved the highest mean crystallinity value of 95% under these optimized operating conditions. Fig. 1 (III) exhibit the crystalline phases of optimized NaAZ (a) and SMZ20 (b). The prominent peaks observed in the pattern Fig. 1 (III, a) provide strong evidence for the formation of highly pure NaAZ. These peaks are particularly intensified at 2θ angles of 7.10°, 10.08°, 12.40°, 16.08°, 21.60°, 24.70°, 27.10°, 29.90°, 34.10°, and 52.54°. As shown in Fig. 1 (III, b), the modification has no impact on the crystalline structure of NaAZ. However, compared to synthesized zeolite, the crystallinity percentage dropped to 90%, indicating that the cationic surfactant was immobilized successfully on the surface of zeolite (Thanos et al., 2012; Choi and Shin, 2020).

FTIR spectroscopy was employed to confirm the structures of synthesized NaAZ, SMZ20, and SMZ20-Gly. Fig. 2 (I) depicts a spectrum with a wavenumber ranging from 400 to 4000 cm^{-1}. The stretching vibration of adsorbed water and O–H groups on the zeolite [Fig. 2 (I, a)] surface is represented by a wide band at 3450 cm^{-1}. The band at 1670 cm^{-1} is attributed to the bending vibrations of water molecules (Davis and Tomozawa, 1996). The FTIR-ART spectra of the T–O bending vibration at 475 cm^{-1}, double ring at 579 cm^{-1}, the single 4-membered rings in the 670 cm^{-1} and the TO_4 antisymmetric stretch at 989 cm^{-1} are considered as evidence of a zeolitic structure formation. The FTIR spectrum of prepared NaAZ was comparable with those previously reported in the literature (Bukhari et al., 2014). Whenever the IR spectrum of the modified sample [Fig. 2 (I, b)] is compared to NaAZ, characteristic peaks are observed at wavenumbers of 2900, 2800, and 1480 cm^{-1} (Bouberka et al., 2009). The bands at around 2800–2900 cm^{-1} indicate symmetric and antisymmetric stretching vibrations of the $–CH_2$ units of the alkyl chain. The immobilization of HDTMAC does not affect the linkage of the Si–O and Al–O bonds in the zeolitic substrate, as evidenced by the presence of vibrations at 475, 579, and 670 cm^{-1} within the crystal structure. However, a noticeable shift in these peaks and an increase in intensities indicate the successful immobilization of HDTMAC on the surface of NaAZ. In addition, the band at about 1480 cm^{-1} was specified for the vibration of the trimethylammonium quaternary group (Noroozi et al., 2018). In the section devoted to the mechanism of adsorption, the FTIR-ATR graph of SMZ20-Gly [Fig. 2 (I, c)] will be discussed in detail.

Zeolite could adsorb water and desorb it from the surface by losing weight in the range of 40–130 °C (Aldahri et al., 2016). Fig. 2 (II) (A&B) compare the TGA-DTG of NaAZ and SMZ20. The weight loss percentage (14.2%) in [Fig. 2 (II, A)] at 120 °C is indicated for the water content removal of NaAZ (Bohra et al., 2014). In [Fig. 2 (II, B)], the first weight loss peak indicated the water removal (3.96%) in the modified zeolite also at 120 °C, which is significantly lower than NaAZ, verifying a lower

Table 1
The chemical composition for AFA, NaAZ and AMZ20 using XRF technique.

Parameters	AFA wt.%	NaAZ	SMZ20
Major oxides			
SiO_2	50.67	32.15	32.15
Al_2O_3	23.20	30.10	30.10
Fe_2O_3	7.73	6.70	6.70
CaO	6.90	5.20	5.20
MgO	2.81	1.68	1.68
K_2O	2.05	2.10	2.10
Na_2O	ND*	18.10	2.5
LOI	3.39	3.39	3.39
Total	96.75	99.42	83.82
SiO_2/Al_2O_3	2.1	1.08	1.08
CEC (meq/100g)	15	435	–
ECEC ((meq/100g)	10	100	–

*Not detectable (ND).

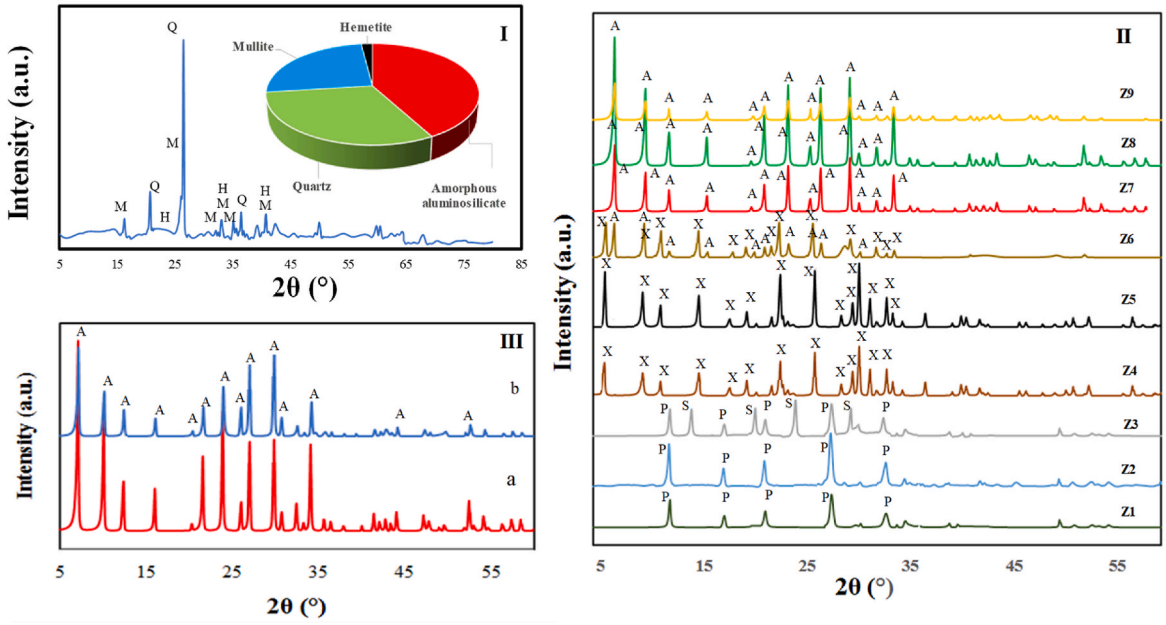

Fig. 1. (I) XRD pattern and quantitative phase analysis of AFA (pie chart), (II) XRD patterns of nine trials by Taguchi model to produce NaAZ (Z1-Z9 from down to top); quartz (Q), mullite (M), NaX (X), NaA (A), NaP1 (P) and SOD (S), and (III) XRD patterns of optimized NaAZ (a) and SMZ20 (b).

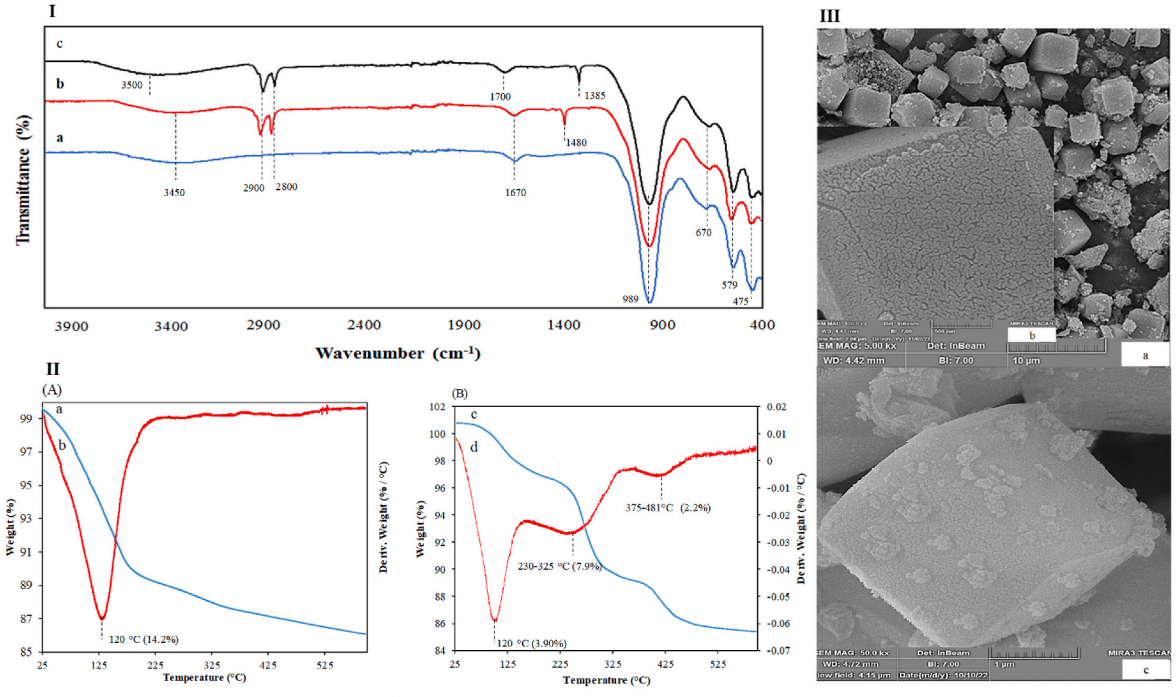

Fig. 2. (I) FTIR-ATR spectra of NaAZ (a), SMZ20 (b) and SMZ20-Gly (c) in the wavelength between 400 and 4000 cm^{-1}. (II) TGA-DTG curves of NaAZ (A) and SMZ20 (B). The falling curves (a, c) represent mass loss throughout the 25–600 °C heating process (50 mL/min N_2 and 10 °C/min) and the temperature marked on the derivative curves (b, d) corresponds to the temperature around which the mass losses occur. (III) SEM images of NaAZ in 10 μm (a), NaAZ surface in 500 nm (b) and SMZ20 in 1 μm (c).

presence of water in the modified zeolite (Dammak et al., 2014). The SMZ20 exhibits secondary decomposition between 230 and 325 °C, as shown by the peak in the derivative curve in [Fig. 2 (II, B, d)]. This could be explained by HDTMAC's hydrophobic-hydrophobic interactions, which implies that the surfactant may be immobilized on the surface of zeolite in a bilayer (Schick et al., 2010). Another difference between unmodified and modified zeolite TGA-DTA curves is the presence of a third mass loss derivative peak between 380 and 450 °C, which is probably attributable to the electrostatic interaction of the ammonium cation head group of HDTMAC with the negative charge of the zeolite surface (Dammak et al., 2015). The modified and unmodified graphs reveal a slight mass loss with a trend to steady when the temperature rises over 500 °C, suggesting that the TGA process is complete.

The SEM morphological analysis of NaAZ and SMZ20 is depicted in

Fig. 2 (III). Cubic zeolite crystal structure [Fig. 2 (III, a)] and a small amount of amorphous phase revealed that NaAZ crystallized on the surface of AFA. Even though the SMZ20 still preserves NaAZ's cubical shape [as shown in Fig. 2 (III, c)], the existence of small, uniform aggregated particles on the surface of SMZ20 is definitive proof that HDTMAC molecules, which are not visible in [Fig. 2 (III, b)], were successfully immobilized on the surface of the zeolite. The results of structural and textural analysis of modified samples showed that surfactant molecules attached to the external surface of zeolites and validate the result of XRD.

SSA, pore volume, and pore diameter measurements could explain NaAZ and SMZ20 textural properties. The NaAZ's SSA declined from 61 m^2/g in NaAZ to 45 m^2/g, indicating that HDTMAC blocked portions of the NaAZ's major channels and reduced N_2 flow (Dávila-Estrada et al., 2018). The SSA of the NaAZ in this experiment were comparable to those of commercial zeolites, which illustrated the synthetic zeolites from AFA was competitive in quality and feasible for further reuse as adsorbents. Pore volume is similarly reduced in NaAZ and SMZ20, respectively, from 0.3 to 0.2 cm^3/g. Long-chain organic surfactant molecules on the zeolite's external layer and at a distance equal to the zeolite super cage's pore openings are responsible for the pore volume reduction. Compared to the SSA and pore volume, the pore diameter follows the opposite trend. Large surfactant molecules with long hydrocarbon tails block pores causing a decrease in the total pore volume and the surface area. NaAZ pore diameter is 4 Å in size, whereas those in the SMZ20 is 14.8 Å. A possible explanation for this result is the presence of a micelle-like macromolecular surfactant on the zeolite's outer surface (Reeve and Fallowfield, 2018).

3.2. Identifying highly effective adsorbent

3.2.1. Effect of pH

pH plays a vital role in adsorbent surface charge changes, Gly deprotonation reactions, and adsorbent speciation (Mohsen Nourouzi et al., 2010; Mamindy-Pajany et al., 2014; Herath et al., 2016b). The adsorption capacity of NaAZ and SMZ20 at different pH values between 2 and 10 was determined. According to the literature, the pKa values for Gly are 0.78, 2.29, 5.96, and 10.90 (Li et al., 2005). Thus, Gly has a positive charge at highly acidic pH values, a neutral charge between 0.78 and 2.29 pH values, and a negative charge above 2.29 pH values that increase with rising pH values (Zhou et al., 2013). As seen in Fig. 1S (A), the maximal adsorption capacity of NaAZ (28 mg/g) was determined at a strongly acidic pH of ~3. The pH_{pzc} might be a crucial parameter to explain the effect of pH on the adsorption process (Mayakaduwa et al., 2016). When the pH of the solution decreases just below the pH_{pzc} in the NaAZ ($pH < 3.3$), the surface of the NaAZ appears positively charged, demonstrating the strong electrostatic interactions with negatively charged groups of Gly molecules at pH values ranging from ~2.29 to 3.3. Then, when the pH of the solution increases, the number of positive charge sites on the NaAZ surface reduces, and the adsorption of Gly diminishes due to the repulsive interaction between the negatively charged adsorbent and the Gly. Consequently, it is assumed that strong electrostatic interactions between positively charged of NaAZ and anionic groups in the Gly molecule are the major mechanism responsible for the maximum Gly adsorption at acidic pH levels. However, it is noteworthy that the pH_{pzc} for SMZ20 [Fig. 1S (B)] was boosted to 6.1, implying that its equilibrium adsorption capacity was improved. The SMZ20 provided a positive net charge in the pH above 3.3 when HDTMAC was attached to the surface of the zeolite. The maximum adoption capacity was found to be 73 mg/g at pH 6, which was achieved by the chemisorption process, which included electrostatic interaction between the positive charge of the amino group in the head of the surfactant and the negative charge of the zeolite's surface. At high $pH > 6.1$ (pH_{pzc}), the density of positive charge sites on the SMZ20 surface decreased, and Gly increased to three negative charges, thereby causing a strong electrostatic repulsion between the negatively charged Gly and SMZ20, resulting in a noticeable decrease in the adsorption. Comparative research was recently published on the adsorption of Gly onto 4A-modified commercial zeolite showed that the highest adsorption capacity was almost 35 mg/g for 100 mg/L Gly at pH 6, which is twice as low as our work (Zavareh et al., 2018). Mayaka and Kumara (Mayakaduwa et al., 2016) demonstrated that woody biochar has ~20 mg/g adsorption capacity for 20 mg/L Gly at pH 6. In another research, the removal efficiency of Gly onto steam-activated woody biochar derived from rice husk was determined to be around 80% at pH 4 (Herath et al., 2016b). Lianna Samuel (Samuel et al., 2017) also showed that when pH increased from 4.2 to 7.7, the removal efficiency increased from 63% to 93%; however, in our project, in the pH 6 the removal efficiency was 95%. Therefore, pH 6 is selected as a neutral or slightly acidic condition to provide favorable conditions for Gly adsorption onto the zeolite surface. The significance of choosing pH 6 for 100 mg/L lies in its relevance to real-world scenarios. pH 6 represents a common range found in various water sources, such as groundwater or industrial effluents. By investigating the adsorption behavior of Gly at pH 6 and a concentration of 100 mg/L, the study aims to simulate and understand the performance of the adsorbent under conditions that closely resemble practical applications. This allows for meaningful comparisons, reliable data interpretation, and potential insights for implementing the adsorption process on a larger scale.

3.2.2. HDTMAC concentrations effect

The application of cationic surfactants in zeolite modification enhances the removal rate of anions by significantly modifying the surface chemistry of minerals (Andrunik et al., 2023). This alteration leads to an increased efficiency in anion removal. The extent of coverage achieved during modification can vary depending on the quantity of surfactant employed. A monolayer of surfactant cations was generated through electrostatic force and cation exchange mechanisms when the concentration of surfactant was equal to or smaller than the CMC (Nezamzadeh-Ejhieh and Raja, 2013). Moreover, the hydrophobic interaction facilitated the attraction of the alkyl chain of the surfactant, promoting bilayer formation when the concentration of the surfactant exceeded the CMC and ECEC. This observation emphasizes the significance of surfactant concentration in enhancing processes such as Gly removal and underscores the relevance of bilayer formation in these mechanisms (Chowdhury et al., 2011). The measurement of the amount of HDTMAC adsorbed onto the NaAZ surface was conducted using the CHN analysis technique. The determination of adsorbed HDTMAC was achieved by comparing the carbon content in the samples before and after modification. The results of this analysis are presented in Table 4S, showing the quantities of loaded and adsorbed HDTMAC, as well as the adsorption efficiency percentage. The examination of these three modified adsorbents was carried out using a Gly solution. As demonstrated in Fig. 2S, there exists a straight association between the surfactant concentration and a noticeable rise in active sites responsible for Gly removal on the zeolite's surface. However, even though a surfactant concentration of 50 mmol/L achieved an efficiency of 97.89% adsorbed HDTMAC, it led to a reduction in the adsorption capacity for Gly removal. This decline indicates an increase in zeolite surface density, potentially resulting in a significant decrease in specific surface area (SSA). This occurrence might be ascribed to micelle formation, causing a decrease in available active sites, as noted by Abbas et al. (2017). Consequently, at a concentration of 20 mmol/L HDTMAC (92.6% adsorption efficiency), SMZ20 emerges as a capable adsorbent with a notably heightened equilibrium adsorption capacity for Gly removal. As a result, SMZ20 has been singled out as an effective adsorbent for subsequent experimental endeavors.

3.3. Optimization of parameters using the Taguchi model

3.3.1. Examining main effect plots

The optimal operating parameters for removing Gly from aqueous solutions using SMZ20 were obtained using a Taguchi L_{16} orthogonal

array experimental design. After 16 trials (triplicate), the results of the mean removal efficiency and S/N ratio variable for each factor at a particular level are shown in Table 5S. In addition, mean effect plots are employed to depict the correlation between factors and output values. The removal efficiency and S/N ratio were boosted when the initial Gly concentration increased from 5 mg/L to 150 mg/L (Fig. 3A), as there were more active sites and more successful Gly molecule collisions in the solution. To surmount the mass transfer resistances of Gly between the aqueous and solid phases, more Gly must be present in the solution. When the concentration was raised over 150 mg/L, there was no discernible enhancement in removal efficiency. It can be concluded that Gly molecules had almost saturated the adsorbent's surface. Comparable effects were seen when Gly was absorbed by different adsorbents, as reported in the literature (Sen et al., 2017, 2019; Sen and Mondal, 2021). Fig. 3B demonstrates the linear correlation between adsorbent dosage (0.1–2 g/L) and Gly removal percentage. High removal efficiency observed with the low adsorbent dosage can be attributed to the combination of a high surface area, surfactant modification, and dosage optimization. These factors synergistically enhance the adsorption capacity and selectivity of the adsorbent, making it a promising and effective solution for Gly removal at a low dosage (Bhaumik and Mondal, 2015). As a result, a smaller quantity of adsorbent is required to achieve the desired Gly removal. This reduction in the required adsorbent volume contributes to overall cost savings, such as lower material procurement and handling expenses. Contact time was the most critical factor in this study, where adsorption rate can interact with Gly molecules and SMZ20. The effect of contact time on Gly adsorption is presented in Fig. 3C. The results reveal that 93% of maximum removal efficiency was recorded at 120 min. After 120 min, the adsorption rate did not change significantly (5%). Such behavior might happen when binding sites are not predominantly occupied, causing a higher collision rate between adsorbate and adsorbent in the presence of a high concentration of Gly molecules with many accessibility sites (Chowdhury et al., 2011).

3.3.2. Statistical analysis of variance (ANOVA)

An ANOVA was performed to assess how much individual variables affected the process's output (in this case, Gly removal efficiency). ANOVA was used to assess the percentage contribution of each operational variable to the response (Googerdchian et al., 2018). The result of the ANOVA for the mean response of removal efficiency is shown in Table 6S. As evidenced by the contribution percentage (P%), contact time (85.82%) > initial concentration (11.87%) > adsorbent dose (1.1%) was shown to be the most influential factor on Gly removal [Fig. 3S (A)]. The P% of the errors was 1.2%, indicating that the tests were carried out under controlled circumstances. Regarding Gly removal efficiency, the coefficient of experimental prediction (R^2-sq) and adjusted coefficient of determination (R^2-adj) was found to be 98.8% and 97.0%, respectively, indicating that the prediction of experimental results was remarkably accurate. The adsorbent dosage is insignificant to removal efficiency, and the time and initial concentration variables are statistically significant (0.05 > P).

3.3.3. Regression plot and confirmation experiment

The linear regression model was employed to establish a connection between SMZ20 process variables and Gly removal efficiency. The validity of the regression model was determined by computing the value of the correlation coefficient. The value of R^2 obtained in this study was 0.9880, which demonstrated a significant agreement between the experimental and predicted dates [shown in Fig. 3S (B)]. The predicted data refers to the values estimated by Taguchi design. The predicted value is calculated based on input variables and the relationship established through data analysis.

In Table 7S, the bolded mean S/N response suggested the optimal level of each component and was regarded as the optimized removal efficiency. The results contribute to the factor combinations of A4, B4, and C4 as the optimal points. In the Taguchi method, a confirmation test is necessary for the optimization study (Elizalde-González and García--Díaz, 2010). Consequently, a triplicate confirmation test revealed that the factor/level combination A4B4C4 has a Gly removal efficiency of 98.92% and a 98.75 mg/g equilibrium adsorption capacity despite not being examined in any of the 16 tests.

3.4. Adsorption kinetic study

The adsorption kinetics data has given crucial information on the

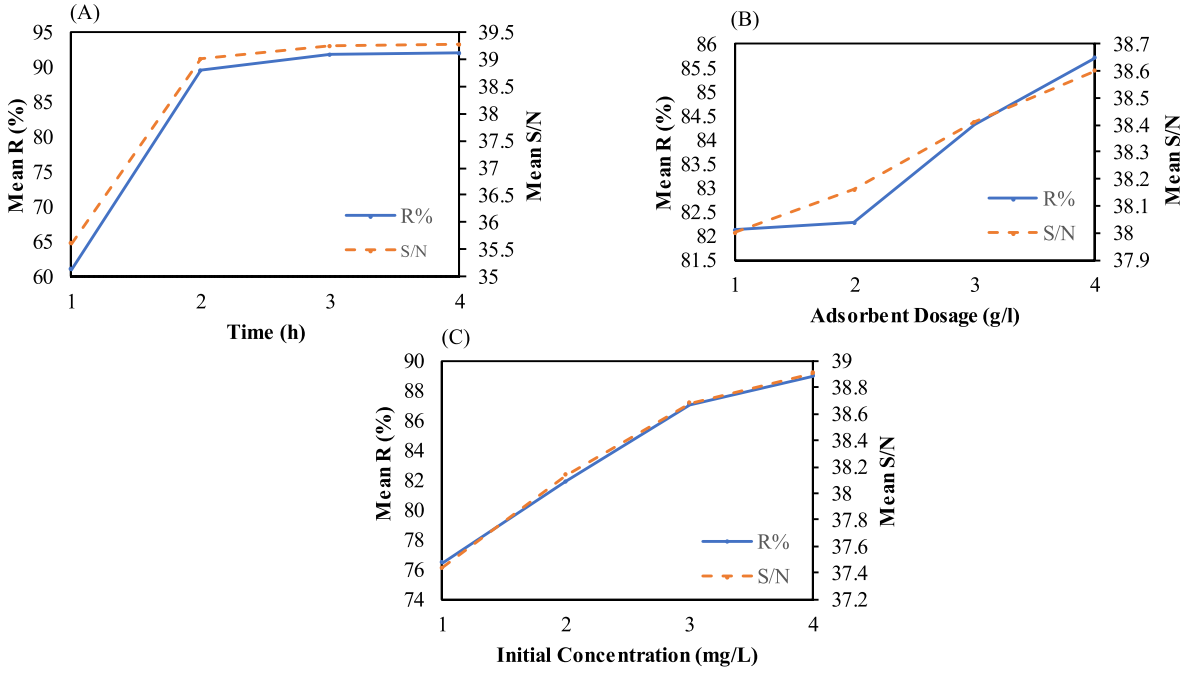

Fig. 3. The mean effect plots for the mean of Gly removal efficiency and S/N ratio in contact time (A), adsorbent dosage (B) and initial concentration (C) using L_{16} Taguchi model in the pH 6.

mechanism of Gly adsorption and the speed at which it occurs on adsorbents. In order to achieve a decent understanding of the mechanism of Gly sorption by the modified zeolite, the data were fitted using the pseudo-first order and pseudo-second order models, which are defined by equations (6) and (7) in Table 2 (Roushani et al., 2017). In the equations, q_t indicates the amount of Gly adsorbed (mg/g) at time t (min), q_e denotes the adsorption capacity of the adsorbent (at equilibrium, mg/g), k_1 implies the pseudo-first order adsorption rate (hr^{-1}), k_2 represents the pseudo-second order adsorption rate (mg/g) constants. As illustrated in Fig. 4A, the compelling achievement of a 93% Gly removal efficiency within a short 2 h contact time, accompanied by a subsequent 5% incremental increase over 24 h, demonstrates the exceptional kinetics of the adsorption process. These significant findings underscore the rapid and efficient nature of Gly removal and highlight the practical implications of our study for time-sensitive applications in water treatment. There is a report of biochar generated from rice husks with comparable equilibrium times (Herath et al., 2016a). In another investigation, MWCNT/MPNs-Fe adsorbent was able to remove 86.23 percent of Gly within 120 min (Diel et al., 2021b). The kinetics result in our investigation validates the contact time results obtained from the Taguchi model. Even though Taguchi's experiment achieved a maximum removal efficiency and adsorption capacity of 24 h, to save cost and energy the benchmark for all other experiments was 2 h. To better comprehend the adsorbent behavior, it should be emphasized that the solute ions rapidly adsorb onto the bulk of the adsorbent as the available active site on the modified zeolite becomes gradually saturated over time. A decrease in sorption was seen as a consequence of the decreasing availability of the positive active sites provided by SMZ20 with increasing time. The pseudo-second order model is predicated on chemical sorption, including electron sharing between the adsorbent and adsorbate (Chowdhury et al., 2011; Ahmad et al., 2018). The calculated R^2 value of 0.9998 (Table 2) indicates that the best match is achieved using a pseudo-second order model, implying a chemisorption mechanism. The pseudo-second order model predicted an adsorption capacity (q_e) of 80 mg/g for Gly sorption onto SMZ20, which is quite close to the experimental result from our investigation. The comparable findings showed that the pseudo second-order model could describe Gly adsorption onto the alum sludge, biopolymer membrane resin D301, $MnFe_2O_4^-$ graphene hybrid composites (Carneiro et al., 2015; Chen et al., 2016; Yamaguchi et al., 2016). To investigate the multiple steps in the adsorption including the diffusion of Gly from the solution phase into the surfaces and subsequently to the pores of SMZ20, the intra-particle diffusion model provided by Weber and Morris (Trinh and Schäfer, 2023) was employed. Intra-particle diffusion could be expressed using equations (8) in Table 2, where q_t is the amount of Gly adsorbed per mass of the SMZ20 (mg/g) at time t, C is related to the thickness of the boundary layer, and k_d is the intra-particle diffusion rate constant (mg/g $min^{0.5}$). Based on the data presented in Fig. 4B, it is evident that the plots of the intra-particle diffusion model exhibit two distinct linear segments, indicating the occurrence of different adsorption processes. In the first process, Gly molecules transfer from the solution and adsorb onto the surface of SMZ20. The second process corresponds to the intra-particle diffusion of Gly molecules from the surface of SMZ20 to the open cavities present within its structure. These findings indicate that the adsorptive removal of Gly is likely influenced by both boundary layer diffusion and intra-particle diffusion. A similar phenomenon was reported by Qingfeng Yang (Yang et al., 2018) in their study on the detection and removal of organophosphorus pesticides using a novel Zr-MOF based smart adsorbent, as well as by Xiangyang Zhu (Zhu et al., 2015) in their research on the removal of organophosphorus pesticides from aqueous solution by Zr-based MOFs of UiO-67. Furthermore, the constant C derived from the intra-particle diffusion model serves as an indicator of whether intra-particle diffusion is the predominant controlling step. A non-zero value of C suggests a complex adsorption mechanism, where multiple factors come into play. On the other hand, if C equals zero, it signifies that the adsorption kinetics are solely governed by intra-particle diffusion. In our study, and in line with most other investigations, the non-zero value of C indicates that the adsorption process follows a complex pathway, influenced by factors beyond intra-particle diffusion alone (Yamaguchi et al., 2016).

Table 2
Isotherm and Kinetic parameters for Gly adsorption onto SMZ20.

Name of model	Equations	Parameter	Value	R_2
Pseudo first order	(6) $q_t = q_e$ [1-exp (-K_1t)]	k_1 (mn^{-1})	0.0207	0.9733
		q_e (mg/g) (model)	71.88	
Pseudo second order	(7) $q_t = (q_e^2K_2t)/1+q_eK_2t$	K_2 (g. $mg^{-1}mn^{-1}$)	0.00055	0.9998
		10^3 q_e model	80	
		q_e (Exp)	78.40	
Intra-particle diffusion	(8) $q_t = k_dt^{0.5}+C$	k_d (mg/g.$h^{0.5}$)	6.723	0.9952
Langmuir	(9) $q_e = q_{max}$ (K_lC_e)/(1+K_lC_e)	q_{max}	769.23	0.9563
		K_l (L/g)	0.01067	
Freundlich	(10) $q_e = K_f C_e^{1/n}$	K_f (mg/g) n	9.1834	0.9942
			1.160	

3.5. Adsorption isotherms

Adsorption isotherms such as the Langmuir and Freundlich isotherms are frequently applied to evaluate the Gly removal mechanism. In the Langmuir model Eq. (8) (Table 2) (Guo et al., 2021), q_{max} (mg/g) is the maximum capacity for Gly's adsorption based on the adsorbent's monolayer coverage, and K_L is the Langmuir constant (L/g), which indicates the energy of adsorption in the adsorption process. In the Freundlich isotherm Eq. (9) (Graziano et al., 2023), the Freundlich constants K_F (mg/g) and n are the relative adsorption capacity and intensity, respectively. For the description of the adsorption behavior of studied SMZ20, correlation coefficients show Fig. 4C that the Freundlich isotherm model is highly appropriate, which points to the presence of the heterogeneous surface. The 'n' value from the Freundlich isotherm represents the degree of nonlinearity between solution concentration and adsorption, whereas a value less than one suggests a chemisorption mechanism and greater than one implies a physical mechanism (Foo and Hameed, 2010). Thus, n suggests that a physical adsorption process between Gly and SMZ20 with a high adsorption intensity occurred in the current investigation (Hameed et al., 2007), which is matched with pseudo-second order kinetics. The Langmuir separation factor, K_L, determines whether a sorption system is irreversible ($K_L = 0$), favorable ($0 < K_L < 1$), linear ($K_L = 1$), or unfavorable ($K_L > 1$). Our K_L value is 0.0106, validating Langmuir model assumptions of favorable sorption. In this study, the Langmuir model simulated a maximum adsorption capacity of 769.23 mg/g. To highlight the performance of the adsorbent employed in the present work in removing the Gly, Table 3 provides a short comparison in terms of maximum adsorption capacity, pH, and removal efficiency with other adsorbents described in the literature. Despite the fact that the findings were obtained under various experimental conditions, there is a significant variance in the maximum adsorption capabilities of several materials, ranging from 3.04 to 769.23 mg/g. Hence, the results of q_{max} and removal efficiency confirm that the developed adsorbent is a feasible, low cost and promising candidate for removing Gly from a water solution. It is noteworthy that by employing a pH closer to its real environment, this novel adsorbent becomes more accurate.

3.6. Adsorption mechanism study

The comprehensive investigation of the adsorption process demonstrated that the adsorption of Gly onto SMZ20 involved a combination of physisorption and chemisorption mechanisms, as supported by the isotherm and kinetics modelling results. The intensity of the adsorbate-adsorbent interaction determined whether the adsorption was characterized by weak physical adsorption or strong chemisorption (Khoury

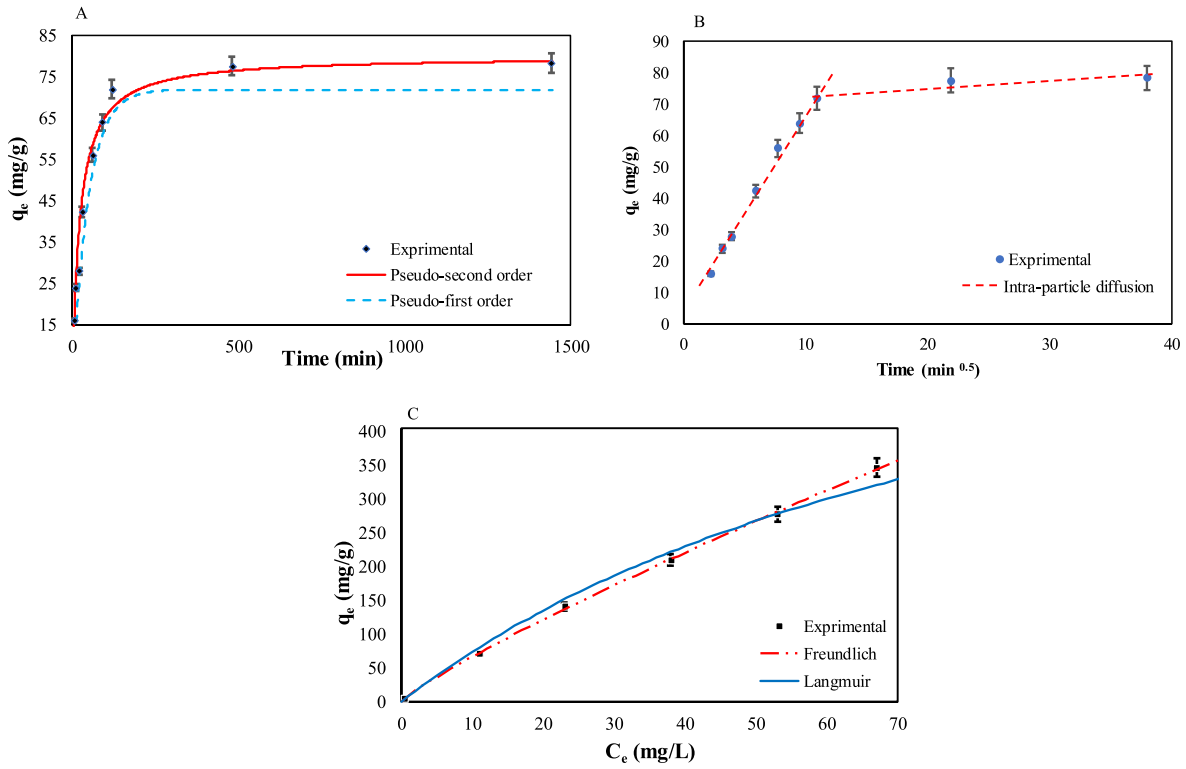

Fig. 4. Experimental kinetics (A), intra-particles diffusion (B) and isotherms (C) data and fitted rate models for adsorption of Gly onto SMZ20.

Table 3
Comparison between SMZ20 and other adsorbents employed in Gly adsorption.

Adsorbents	Removal efficiency (%)	q_{max} (mg/g)	pH	Ref.
MWCNT/MPNs-Fe	86.23	43.66	4	Diel et al. (2021)
Thiol modified magMCM-41 nanoparticles	79.38	106.38	5	Zadeh et al. (2021)
(TMC)-silica hybrid shells-Fe_3O_4	97	3.04	5	Soares et al. (2021)
D301 resin	–	392.2	<7	Wang et al. (2021)
Cu-zeolite 4A	80	112.7	6	Zavareh et al. (2018)
Hierarchical porous UiO-67	–	322.58	7	Fang et al. (2022)
Rice husk derived engineered biochar	82.0	123.03	4	Herath et al. (2016)
Dendrimer functionalized	95	14.04	5	Guo et al. (2019)
Lignin/Fe_3O_4/La $(OH)_3$	97	83.87	>5	Li et al. (2021)
Fe_3O_4@SiO_2@UiO-67	–	256.54	4	Yang et al. (2018)
CS-CNC@UiO-66-NH_2	–	133.7	4	Luo et al. (2021)
chitosan/alginate combination	–	8.70	6.5	Carneiro et al. (2015)
HUiO-66s	–	400	6	Tao et al. (2022)
SMZ20	98.92	769.23	6	This work

et al., 2010). H-bonding was observed during physisorption, while chemisorption was associated with electrophilic interactions (Herath et al., 2016a). To illustrate the possible mechanisms of Gly adsorption onto SMZ20 at pH 6.0, a graphical representation was provided in Fig. 5. Several potential mechanisms were postulated. Firstly, at pH values below the point of zero charge (pHpzc), the protonation of Gly residues, particularly the phosphate and carbocyclic groups, resulted in the

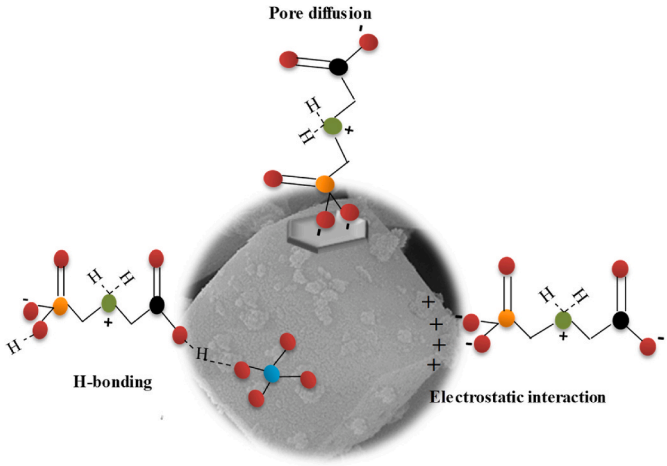

Fig. 5. Mechanisms of Gly removal using SMZ20 as an efficient adsorbent.

formation of a strong electrophile. This allowed for the interaction with the positively charged "head" of HDTMAC on both the inner and outer layers and the micelles, leading to chemisorption. Secondly, the findings from the FTIR-ATR analysis supported our observations. The reduced peak intensities in the modified zeolite after Gly adsorption, as shown in Fig. 2 (I, c), indicated the interaction between the modified zeolite and Gly. The shifting of the OH peaks from 3450 to 3500 and 1670 to 1700 suggested the formation of H-bonding between Gly and the modified zeolite. Additionally, the peaks observed at 1385 cm^{-1} could be attributed to the vibration of carboxyl functional groups of Gly (Liu et al., 2022). Furthermore, pore diffusion was identified as a potential adsorption mechanism in the porous material. The pore diameter of the adsorbent, which measured approximately twice the size of the Gly molecule [7.14 Å × 2.68 Å × 3.02 Å (Rojas and Horcajada, 2020)], suggests the possibility of pore diffusion in this study. This hypothesis

could be validated by the outcomes of the intra-particle pore diffusion mechanism. This implies that Gly molecules can diffuse into the adsorbent's pores, facilitating their adsorption. The detailed understanding of the adsorption mechanisms reveals that the modified adsorbent exhibits both physisorption and chemisorption, allowing for stronger and more effective interactions with Gly molecules. This translates into a higher adsorption capacity compared to conventional adsorbents, offering improved efficiency in removing Gly from water solutions. The presence of specific functional groups on the modified adsorbent's surface enables selective adsorption of Gly. In conclusion, the significant application of the modified adsorbent lies in its enhanced adsorption capacity, selective adsorption, pH-dependent behavior, and versatile application potential. The deep understanding of the underlying adsorption mechanisms sets the modified adsorbent apart, offering a novel and promising solution for the efficient removal of Gly and potentially other organic contaminants from water sources.

4. Leaching determination

4.1. Leaching of heavy metals

The high concentration of heavy metals in waste CFA poses a potential threat to animal and human health as well as the environment. By effectively reducing the leaching of heavy metals, the NaAZ and SMZ20 play a crucial role in protecting ecosystems and safeguarding water and soil quality (Bukhari et al., 2016). Se, Pb, and Mn concentrations in the leachate elements from AFA, NaAZ and SMZ20 into the solution through the DIN leaching test were determined to be under the reportable threshold, as shown in Table 8S. The NaAZ and SMZ20 exhibited a significant decrease in the concentrations of cationic metals such as B, Cr, Co, Cu, Mg, Ni, and V compared to AFA. This reduction indicates that the incorporation of these metals into the zeolites structure effectively immobilizes them, preventing their leaching into the environment and mitigating potential environmental risks. The leachate experiments revealed that anionic species, including arsenic anions, tend to leach out of the NaAZ. However, the modified zeolites exhibited a significant reduction in the concentration of these anions, indicating that the SMZ20, facilitates electrostatic interactions that help retain anionic species and prevent their leaching. Thus, the use of the SMZ20 demonstrates significant justifications in terms of environmental and health protection, reduction of cationic metal leaching and prevention of anionic species leaching. These reasons highlight the importance and effectiveness of the modified zeolite in preventing heavy metal leaching from waste AFA and its potential as a sustainable solution for managing and mitigating heavy metal contamination.

4.2. Leaching of adsorbed Gly

The leaching time significantly influences the mobility of adsorbed Gly from the adsorbents into the solution. The data in Table 4 demonstrate that NaAZ released nearly all of the adsorbed Gly within 60 days, while the modified zeolite only leached a minimal amount of 6 ppm of adsorbed Gly after the same period. The strong chemical and physical interactions between Gly and the modified zeolite can be attributed to the low leaching observed. The adsorbed HDTMAC molecules, located at cation-exchange sites, form strong bonds with the surface of the NaAZ, preventing easy displacement by water or leaching. These interactions contribute to the enhanced stability of the Gly adsorbed onto the SMZ20. These justifications highlight the practical significance of using the SMZ20 for adsorption applications, where the retention and stability of the adsorbed species are crucial factors to consider.

5. Conclusions

This study demonstrates the effective reuse of AFA for environmentally eco-friendly synthesis of NaAZ, with optimized conditions ($NaAl_2O_3$ 0.5 M, AFA/NaOH ratio of 1:2, temperature 85 °C and duration 6 h) yielding a high crystallinity of 93%. Crystallized NaAZ was then modified with HDTMAC surfactant and implemented as a novel application for Gly removal from water solution. Due to the varied pK_a values of Gly, pH was a critical factor in Gly elimination. Enhancing the pH_{pzc} from 3.3 in the NaAZ to 6.1 in the SMZ20 was a noteworthy achievement of this research to improve the equilibrium adsorption capacity. The Taguchi method was employed to optimize the batch adsorption test for Gly removal, resulting in impressive outcomes of 98.75 mg/g equilibrium adsorption capacity and 98.92% removal efficiency. The optimal parameters, including 2 g/L adsorbent dosage, 200 mg/L Gly initial concentration, and 24 h contact time, contributed to these remarkable results. This study validated the proposed adsorption mechanisms of electrostatic interaction, pore diffusion, and H-bonding through comprehensive analysis of FTIR-ATR characterization, kinetics, and isotherm data. Based on the Langmuir isotherm model, the adsorption capacity of SMZ20 for Gly was determined to be 769.23 mg/g, indicating its exceptional performance and consistency with previous research findings. Remarkably, the leaching experiment demonstrated the effective retention of Gly by the SMZ20, with a low concentration of 6 ppm observed after 60 days. This highlights the stability and durability of the adsorbent material, making it suitable for environmental applications. Furthermore, NaAZ and SMZ20 effectively reduce the levels of hazardous heavy metals. The SMZ20 significantly minimizes As leaching into the solution compared to AFA and NaAZ supernatants, highlighting its environmental significance. Consequently, the findings demonstrated that the SMZ20 is a practical, inexpensive, and innovative adsorbent for removing Gly that might be considered a promising candidate for environmental remediation in the future.

Table 4
Leaching of Gly from NaAZ-Gly and SMZ20-Gly.

Time (day)	Leachate Gly from NaAZ-Gly (ppm)	Leachate Gly from SMZ20-Gly (ppm)
1	16	4
30	19	7
60	25	6

Credit author statement

Sarah Haghjoo: Resources, Investigation, Roles/Writing - original draft. Christian L. Lengauer: Supervision, Conceptualization, Methodology, Validation, Funding acquisition, Writing - review &editing. Hossein Kazemian: Supervision, Conceptualization, Corresponding author, Methodology, Validation, Funding acquisition, Writing - review &editing. Mahmoud Roushani: Data curation, Validation, Visualization, Methodology, Writing - review &editing.

Declaration of competing interest

The authors declare that they have no known competing financial interests or personal relationships that could have appeared to influence the work reported in this paper.

Data availability

Data will be made available on request.

Acknowledgement

The authors would like to express their sincere gratitude to the Marietta Blau funding, generously provided by the Austrian Federal Ministry of Education, Science and Research (BMBWF). Special appreciation is extended to the dedicated analytical lab specialists from the Northern Analytical Lab Services at the University of Northern British

Columbia for their invaluable technical support during the course of this study. Additionally, H. Kazemian acknowledges with heartfelt thanks the support extended by the Natural Sciences and Engineering Research Council of Canada (NSERC) through the Discovery Grant, bearing the funding reference number RGPIN-2019-06304. Their contributions have been instrumental in the successful execution of this research.

Appendix A. Supplementary data

Supplementary data to this article can be found online at https://doi.org/10.1016/j.jenvman.2023.118976.

References

Abbas, A., Sallam, A.S., Usman, A.R., Al-Wabel, M.I., 2017. Organoclay-based nanoparticles from montmorillonite and natural clay deposits: synthesis, characteristics, and application for MTBE removal. Appl. Clay Sci. 142, 21–29.
Ahmad, A.L., Lah, N.F.C., Low, C., 2018. Configuration of molecular imprinted polymer for electrochemical atrazine detection. L. J. Polym. Res. 25, 1–9.
Aldahri, T., Behin, J., Kazemian, H., Rohani, S., 2016. Synthesis of zeolite Na-P from coal fly ash by thermo-sonochemical treatment. Fuel 182, 494–501.
Aldahri, T., Behin, J., Kazemian, H., Rohani, S., 2017. Effect of microwave irradiation on crystal growth of zeolitized coal fly ash with different solid/liquid ratios. Adv. Powder Technol. 28, 2865–2874.
Ameh, A.E., Fatoba, O.O., Musyoka, N.M., Petrik, L.F., 2017. Influence of aluminium source on the crystal structure and framework coordination of Al and Si in fly ash-based zeolite NaA. Powder Technol. 306, 17–25.
Anbia, M., Mohammadi Nejati, F., Jahangiri, M., Eskandari, A., Garshasbi, V., 2015. Optimization of synthesis procedure for NaX Zeolite by Taguchi experimental design and its application in CO_2 adsorption. J. Sci. Islam. Repub. Iran 26, 213–222.
Andrunik, M., Skalny, M., Bajda, T., 2023. Functionalized adsorbents resulting from the transformation of fly ash: characterization, modification, and adsorption of pesticides. Separ. Purif. Technol., 123106
Arroyave, J.M., Waiman, C.C., Zanini, G.P., Avena, M.J., 2016. Effect of humic acid on the adsorption/desorption behavior of glyphosate on goethite. Isotherms and kinetics. Chemosphere 145, 34–41.
Asl, S.M.H., Ghadi, A., Baei, M.S., Javadian, H., Maghsudi, M., Kazemian, H., 2018. Porous catalysts fabricated from coal fly ash as cost-effective alternatives for industrial applications: a review. Fuel 217, 320–342.
Attari, M., Bukhari, S.S., Kazemian, H., Rohani, S., 2017. A low-cost adsorbent from coal fly ash for mercury removal from industrial wastewater. J. Environ. Chem. Eng. 5, 391–399.
Battaglin, W.A., Rice, K.C., Focazio, M.J., Salmons, S., Barry, R.X.J.E.M., Assessment, 2009. The occurrence of glyphosate, atrazine, and other pesticides in vernal pools and adjacent streams in Washington, DC, Maryland, Iowa, and Wyoming, 2005–2006. Environ. Monit. Assess. 155, 281–307.
Bhaumik, R., Mondal, N.K., 2015. Adsorption of fluoride from aqueous solution by a new low-cost adsorbent: thermally and chemically activated coconut fibre dust. Clean Technol. Environ. Policy 17, 2157–2172.
Bohra, S., Kundu, D., Naskar, M.K., 2014. One-pot synthesis of NaA and NaP zeolite powders using agro-waste material and other low cost organic-free precursors. Ceram. Int. 40, 1229–1234.
Bouberka, Z., Khenifi, A., Mahamed, H.A., Haddou, B., Belkaid, N., Bettahar, N., 2009. Adsorption of Supranol Yellow 4 GL from aqueous solution by surfactant-treated aluminum/chromium-intercalated bentonite. J. Hazard Mater. 162, 378–385.
Bukhari, S.S., Behin, J., Kazemian, H., Rohani, S., 2014. A comparative study using direct hydrothermal and indirect fusion methods to produce zeolites from coal fly ash utilizing single-mode microwave energy. J. Mater. Sci. 49, 8261–8271.
Bukhari, S.S., Behin, J., Kazemian, H., Rohani, S., 2015. Conversion of coal fly ash to zeolite utilizing microwave and ultrasound energies: a review. Fuel 140, 250–266.
Bukhari, S.S., Rohani, S., Kazemian, H., 2016. Effect of ultrasound energy on the zeolitization of chemical extracts from fused coal fly ash. Ultrason. Sonochem. 28, 47–53.
Carneiro, R.T., Taketa, T.B., Neto, R.J.G., Oliveira, J.L., Campos, E.V., de Moraes, M.A., da Silva, C.M., Beppu, M.M., L F J J o e m, Fraceto, 2015. Removal of glyphosate herbicide from water using biopolymer membranes. J. Environ. Manag. 151, 353–360.
Cederlund, H., Börjesson, E., Stenström, J., 2017. Effects of a wood-based biochar on the leaching of pesticides chlorpyrifos, diuron, glyphosate and MCPA. J. Environ. Manag. 191, 28–34.
Chaves, T.F., Pastore, H.O., Cardoso, D.J.M., materials, m., 2012. A simple synthesis procedure to prepare nanosized faujasite crystals. Microporous Mesoporous Mater. 161, 67–75.
Chen, F.-x., Zhou, C.-r., Li, G.-p., Peng, F., 2016. Thermodynamics and kinetics of glyphosate adsorption on resin D301. Arab. J. Chem. 9, S1665–S1669.
Choi, J., Shin, W.S.J.M., 2020. Removal of salicylic and ibuprofen by hexadecyltrimethylammonium-modified montmorillonite and zeolite. Minerals 10, 898.
Chowdhury, S., Mishra, R., Saha, P., Kushwaha, P., 2011. Adsorption thermodynamics, kinetics and isosteric heat of adsorption of malachite green onto chemically modified rice husk. Desalination 265, 159–168.
Chutia, P., Kato, S., Kojima, T., Satokawa, S., 2009. Adsorption of as (V) on surfactant-modified natural zeolites. J. Hazard Mater. 162, 204–211.
Crocker, F.H., Guerin, W.F., Boyd, S., technology, 1995. Bioavailability of naphthalene sorbed to cationic surfactant-modified smectite clay. Environ. Sci. Technol. 29, 2953–2958.
Dammak, N., Ouledltaief, O., Fakhfakh, N., Benzina, M., 2014. Adsorption equilibrium studies for O-xylene vapour and modified clays system. Surf. Interface Anal. 46, 457–464.
Dammak, N., Fakhfakh, N., Fourmentin, S., Benzina, M., 2015. Treatment of gas containing hydrophobic VOCs by adsorption process on raw and intercalated clays. Res. Chem. Intermed. 41, 5475–5493.
Dargahi, M., Kazemian, H., Soltanieh, M., Hosseinpour, M., Rohani, S., 2012. High temperature synthesis of SAPO-34: applying an L9 Taguchi orthogonal design to investigate the effects of experimental parameters. Powder Technol. 217, 223–230.
Dávila-Estrada, M., Ramírez-García, J.J., Solache-Ríos, M.J., Gallegos-Pérez, J.L., 2018. Kinetic and equilibrium sorption studies of ceftriaxone and paracetamol by surfactant-modified zeolite. Water, Air, Soil Pollut. 229, 1–9.
Davis, K., Tomozawa, M., 1996. An infrared spectroscopic study of water-related species in silica glasses. J. Non-Cryst. Solids 201, 177–198.
de Aquino, T.F., Estevam, S.T., Viola, V.O., Marques, C.R., Zancan, F.L., Vasconcelos, L. B., Riella, H.G., Pires, M.J., Morales-Ospino, R., Torres, A.E.B., 2020. CO2 adsorption capacity of zeolites synthesized from coal fly ashes. Fuel 276, 118143.
Diel, J.C., Franco, D.S., Nunes, I.d.S., Pereira, H.A., Moreira, K.S., Thiago, A.d.L., Foletto, E.L., Dotto, G.L., 2021. Carbon nanotubes impregnated with metallic nanoparticles and their application as an adsorbent for the glyphosate removal in an aqueous matrix. J. Environ. Chem. Eng. 9, 105178.
Diel, J.C., Franco, D.S., Igansi, A.V., Cadaval Jr., T.R., Pereira, H.A., Nunes, I.d.S., Basso, C.W., Maria do Carmo, M.A., Morais, J., Pinto, D., 2021a. Green synthesis of carbon nanotubes impregnated with metallic nanoparticles: characterization and application in glyphosate adsorption. Chemosphere 283, 131193.
Diel, J.C., Franco, D.S., Nunes, I.d.S., Pereira, H.A., Moreira, K.S., Thiago, A.d.L., Foletto, E.L., Dotto, G.L., 2021b. Carbon nanotubes impregnated with metallic nanoparticles and their application as an adsorbent for the glyphosate removal in an aqueous matrix. J. Environ. Chem. Eng. 9, 105178.
Do, M.H., Florea, A., Farre, C., Bonhomme, A., Bessueille, F., Vocanson, F., Tran-Thi, N.-T., Jaffrezic-Renault, N., 2015. Molecularly imprinted polymer-based electrochemical sensor for the sensitive detection of glyphosate herbicide. Int. J. Environ. Anal. Chem. 95, 1489–1501.
El-Naggar, M., El-Kamash, A., El-Dessouky, M., Ghonaim, A., 2008. Two-step method for preparation of NaA-X zeolite blend from fly ash for removal of cesium ions. J. Hazard Mater. 154, 963–972.
Elizalde-González, M., García-Díaz, L., 2010. Application of a Taguchi L16 orthogonal array for optimizing the removal of Acid Orange 8 using carbon with a low specific surface area. Chem. Eng. J. 163, 55–61.
Fang, F., Lv, Q., Li, P., Tao, Y., Zhang, Y., Zhou, Y., Li, X., Li, J., 2022. Screening of hierarchical porous UiO-67 for efficient removal of glyphosate from aqueous solution. J. Environ. Chem. Eng. 10, 107824.
Foo, K.Y., Hameed, B.H., 2010. Insights into the modeling of adsorption isotherm systems. Chem. Eng. J. 156, 2–10.
Ghiaci, M., Abbaspur, A., Kia, R., Seyedeyn-Azad, F.J.S., technology, p., 2004. Equilibrium isotherm studies for the sorption of benzene, toluene, and phenol onto organo-zeolites and as-synthesized MCM-41. Separ. Purif. Technol. 40, 217–229.
Googerdchian, F., Moheb, A., Emadi, R., Asgari, M., 2018. Optimization of Pb (II) ions adsorption on nanohydroxyapatite adsorbents by applying Taguchi method. J. Hazard Mater. 349, 186–194.
Graziano, M., Porfiri, C., Tufo, A.E., Montoya, J.C., dos Santos Afonso, M., 2023. Reversibility of glyphosate sorption in pampean loess-derived soil profiles of central Argentina. Chemosphere 312, 137143.
Guo, D., Muhammad, N., Lou, C., Shou, D., Y J N J o C, Zhu, 2019. Synthesis of dendrimer functionalized adsorbents for rapid removal of glyphosate from aqueous solution 43, 121–129.
Guo, F., Zhou, M., Xu, J., Fein, J.B., Yu, Q., Wang, Y., Huang, Q., Rong, X., 2021. Glyphosate adsorption onto kaolinite and kaolinite-humic acid composites: experimental and molecular dynamics studies. Chemosphere 263, 127979.
Haggerty, G.M., Bowman, R.S., 1994. Sorption of chromate and other inorganic anions by organo-zeolite. Environ. Sci. Technol. 28, 452–458.
Hailu, S.L., Nair, B.U., Redi-Abshiro, M., Diaz, I., Tessema, M., 2017. Preparation and characterization of cationic surfactant modified zeolite adsorbent material for adsorption of organic and inorganic industrial pollutants. J. Environ. Chem. Eng. 5, 3319–3329.
Hameed, B., Din, A.M., Ahmad, A., 2007. Adsorption of methylene blue onto bamboo-based activated carbon: kinetics and equilibrium studies. J. Hazard Mater. 141, 819–825.
Herath, I., Kumarathilaka, P., Al-Wabel, M.I., Abduljabbar, A., Ahmad, M., Usman, A.R., Vithanage, M.J.M., materials, m., 2016. Mechanistic modeling of glyphosate interaction with rice husk derived engineered biochar 225, 280–288.
Herath, I., Kumarathilaka, P., Al-Wabel, M.I., Abduljabbar, A., Ahmad, M., Usman, A.R., Vithanage, M., 2016a. Mechanistic modeling of glyphosate interaction with rice husk derived engineered biochar. Microporous Mesoporous Mater. 225, 280–288.
Herath, I., Kumarathilaka, P., Al-Wabel, M.I., Abduljabbar, A., Ahmad, M., Usman, A.R., Vithanage, M.J.M., materials, m., 2016b. Mechanistic modeling of glyphosate interaction with rice husk derived engineered biochar. Microporous Mesoporous Mater. 225, 280–288.
Hu, Y., Zhao, Y., Sorohan, B.J.D., 2011. Removal of glyphosate from aqueous environment by adsorption using water industrial residual. Desalination 271, 150–156.

Kazi, T., Jamali, M., Kazi, G., Arain, M., Afridi, H., Siddiqui, A., 2005. Evaluating the mobility of toxic metals in untreated industrial wastewater sludge using a BCR sequential extraction procedure and a leaching test. Anal. Bioanal. Chem. 383, 297–304.
Khoury, G.A., Gehris, T.C., Tribe, L., Sánchez, R.M.T., dos Santos Afonso, M.J.A.C.S., 2010. Glyphosate adsorption on montmorillonite: an experimental and theoretical study of surface complexes. Appl. Clay Sci. 50, 167–175.
Li, Z., Bowman, R.S.J.E.S., Technology, 1998. Sorption of perchloroethylene by surfactant-modified zeolite as controlled by surfactant loading. Environ. Sci. Technol. 32, 2278–2282.
Li, F., Wang, Y., Yang, Q., Evans, D.G., Forano, C., Duan, X.J., 2005. Study on adsorption of glyphosate (N-phosphonomethyl glycine) pesticide on MgAl-layered double hydroxides in aqueous solution. J. Hazard Mater. 125, 89–95.
Li, C., Li, Y., Li, Q., Duan, J., Hou, J., Hou, Q., Ai, S., Li, H., Yang, Y., 2021. Regenerable magnetic aminated lignin/Fe3O4/La (OH) 3 adsorbents for the effective removal of phosphate and glyphosate. Sci. Total Environ. 788, 147812.
Liang, Y., Wei, D., Hu, J., Zhang, J., Liu, Z., Li, A., Li, R.J.W.r., 2020. Glyphosate and nutrients removal from simulated agricultural runoff in a pilot pyrrhotite constructed wetland. Water Res. 168, 115154.
Liu, M., Hou, L.-a., Yu, S., Xi, B., Zhao, Y., Xia, X.J.C.e.j., 2013. MCM-41 impregnated with A zeolite precursor: synthesis, characterization and tetracycline antibiotics removal from aqueous solution. Chem. Eng. J. 223, 678–687.
Liu, R., Xie, Y., Cui, K., Xie, J., Zhang, Y., Huang, Y., 2022. Adsorption behavior and adsorption mechanism of glyphosate in water by amino-MIL-101 (Fe). J. Phys. Chem. Solid. 161, 110403.
Luo, X., Huang, G., Chen, X., Guo, J., Yang, W., Tang, W., Yue, T., Li, Z., 2021. Ingenious ambient temperature fabrication zirconium-metal organic framework laden polysaccharide aerogel as an efficient glyphosate scavenger. J. Environ. Chem. Eng. 9, 106808.
Mamindy-Pajany, Y., Sayen, S., Mosselmans, J.F.W., Guillon, E.J.E.s., 2014. Copper, nickel and zinc speciation in a biosolid-amended soil: pH adsorption edge, μ-XRF and μ-XANES investigations. Environ. Sci. Technol. 48, 7237–7244.
Mayakaduwa, S., Kumarathilaka, P., Herath, I., Ahmad, M., Al-Wabel, M., Ok, Y.S., Usman, A., Abduljabbar, A., Vithanage, M.J.C., 2016. Equilibrium and kinetic mechanisms of woody biochar on aqueous glyphosate removal. Chemosphere 144, 2516–2521.
Milojević-Rakić, M., Popadić, D., Ležaić, A.J., Jevremović, A., Vasiljević, B.N., Uskoković-Marković, S., Bajuk-Bogdanović, D., 2022. MFI, BEA and FAU zeolite scavenging role in neonicotinoids and radical species elimination. Environmental Science: Process. Impacts 24, 265–276.
Mohsen Nourouzi, M., Chuah, T., Choong, T.S.J.D., Treatment, W., 2010. Adsorption of glyphosate onto activated carbon derived from waste newspaper. Desalination Water Treat. 24, 321–326.
Myers, J.P., Antoniou, M.N., Blumberg, B., Carroll, L., Colborn, T., Everett, L.G., Hansen, M., Landrigan, P.J., Lanphear, B.P., Mesnage, R., 2016. Concerns over use of glyphosate-based herbicides and risks associated with exposures: a consensus statement. Environ. Health 15, 1–13.
Nargis, F., Duong, A., Rehl, E., Bradshaw, C., Kazemian, H., 2022. Highly efficient and low-cost clay-based adsorbent for glyphosate removal from contaminated water. Chem. Eng. Technol. 45, 340–347.
Nezamzadeh-Ejhieh, A., Raja, G., 2013. Modification of nanoclinoptilolite zeolite with hexadecyltrimethylammonium surfactant as an active ingredient of chromate-selective membrane electrode. J. Chem. 2013.
Noroozi, R., Al-Musawi, T.J., Kazemian, H., Kalhori, E.M., Zarrabi, M., 2018. Removal of cyanide using surface-modified Linde Type-A zeolite nanoparticles as an efficient and eco-friendly material. J. Water Proc. Eng. 21, 44–51.
Pankajakshan, A., Sinha, M., Ojha, A.A., Mandal, S., 2018. Water-stable nanoscale zirconium-based metal–organic frameworks for the effective removal of glyphosate from aqueous media. ACS Omega 3, 7832–7839.
Reeve, P.J., Fallowfield, H.J., 2018. Natural and surfactant modified zeolites: a review of their applications for water remediation with a focus on surfactant desorption and toxicity towards microorganisms. J. Environ. Manag. 205, 253–261.
Rojas, S., Horcajada, P., 2020. Metal–organic frameworks for the removal of emerging organic contaminants in water. Chem. Rev. 120, 8378–8415.
Roushani, M., Saedi, Z., Baghelani, Y.M., 2017. Removal of cadmium ions from aqueous solutions using TMU-16-NH2 metal organic framework. Environ. Nanotechnol. Monit. Manag. 7, 89–96.
Ruen-ngam, D., Rungsuk, D., Apiratikul, R., Pavasant, P., Association, W.M., 2009. Zeolite formation from coal fly ash and its adsorption potential. J. Air Waste Manag. Assoc. 59, 1140–1147.
Samuel, L., Wang, R., Dubois, G., Allen, R., Wojtecki, R., La, Y.-H., 2017. Amine-functionalized, multi-arm star polymers: a novel platform for removing glyphosate from aqueous media. Chemosphere 169, 437–442.
Schick, J., Caullet, P., Paillaud, J.-L., Patarin, J., Mangold-Callarec, C., 2010. Batch-wise nitrate removal from water on a surfactant-modified zeolite. Microporous Mesoporous Mater. 132, 395–400.
Sen, K., Mondal, N.K., 2021. Statistical optimization of glyphosate adsorption by silver nanoparticles loaded activated carbon: kinetics, isotherms and thermodynamics. Environ. Nanotechnol. Monit. Manag. 16, 100547.
Sen, K., Mondal, N.K., Chattoraj, S., Datta, J.K., 2017. Statistical optimization study of adsorption parameters for the removal of glyphosate on forest soil using the response surface methodology. Environ. Earth Sci. 76, 1–15.
Sen, K., Datta, J.K., Mondal, N.K., 2019. Glyphosate adsorption by Eucalyptus camaldulensis bark-mediated char and optimization through response surface modeling. Appl. Water Sci. 9, 1–12.
Sittiwong, J., Hiruntrakool, K., Rasrichai, A., Opasmongkolchai, O., Srifa, P., Nilwanna, K., Maihom, T., Probst, M., Limtrakul, J., 2022. Insights into glyphosate adsorption on Lewis acidic zeolites from theoretical modelling. Microporous Mesoporous Mater. 341, 112083.
Soares, S.F., Amorim, C.O., Amaral, J.S., Trindade, T., Daniel-da-Silva, A.L., 2021. On the efficient removal, regeneration and reuse of quaternary chitosan magnetite nanosorbents for glyphosate herbicide in water. J. Environ. Chem. Eng. 9, 105189.
Tao, Y., Fang, F., Lv, Q., Qin, W., He, X., Zhang, Y., Zhou, Y., Li, X., Li, J., 2022. Highly efficient removal of glyphosate from water by hierarchical-pore UiO-66: selectivity and effects of natural water particles. J. Environ. Manag. 316, 115301.
Thanos, A., Katsou, E., Malamis, S., Psarras, K., Pavlatou, E., Haralambous, K.J.C.e.j., 2012. Evaluation of modified mineral performance for chromate sorption from aqueous solutions. Chem. Eng. J. 211, 77–88.
Trinh, P.B., Schäfer, A.I., 2023. Adsorption of glyphosate and metabolite aminomethylphosphonic acid (AMPA) from water by polymer-based spherical activated carbon (PBSAC). J. Hazard Mater. 454, 131211.
Wang, S., Peng, Y.J.C.e.j., 2010. Natural zeolites as effective adsorbents in water and wastewater treatment. Chem. Eng. J. 156, 11–24.
Wang, M., Rivenbark, K.J., Phillips, T.D., 2024. Kinetics of glyphosate and aminomethylphosphonic acid sorption onto montmorillonite clays in soil and their translocation to genetically modified corn. J. Environ. Sci. 135, 669-680.
Wang, Y., Guo, Y., Yang, Z., Cai, H., Xavier, Q., 2003. Synthesis of zeolites using fly ash and their application in removing heavy metals from waters. Sci. China Earth Sci. 46, 967–976.
Wang, Y., Guo, Y.-p., Li, H.-x., Zhou, R.-y., Yu, J.-x., Hou, H.-b., Yin, W., R-A J J o E C E, Chi, 2021. Sequential recycle of valuable phosphorus compounds of glyphosine, glyphosate, and phosphorous acid from glyphosate mother liquor by D301 resin through sorbent dosage control 9, 106474.
Xie, Y., Xiong, R., Li, J., Li, W., Yang, X., Tong, H., 2023. Insight into n-CaO2/SBC/Fe (II) Fenton-like system for glyphosate degradation: pH change, iron conversion, and mechanism. J. Environ. Manag. 333, 117428.
Yamaguchi, N.U., Bergamasco, R., Hamoudi, S.J.C.E.J., 2016. Magnetic MnFe2O4–graphene hybrid composite for efficient removal of glyphosate from water. Chem. Eng. J. 295, 391–402.
Yang, Q., Wang, J., Chen, X., Yang, W., Pei, H., Hu, N., Li, Z., Suo, Y., Li, T., Wang, J., 2018. The simultaneous detection and removal of organophosphorus pesticides by a novel Zr-MOF based smart adsorbent. J. Mater. Chem. A 6, 2184–2192.
Yi, H., Deng, H., Tang, X., Yu, Q., Zhou, X., Liu, H., 2012. Adsorption equilibrium and kinetics for SO2, NO, CO2 on zeolites FAU and LTA. J. Hazard Mater. 203, 111–117.
Zadeh, R.J., Sayadi, M.H., Rezaei, M.R., 2021. Synthesis of Thiol modified magMCM-41 nanoparticles with rice husk ash as a robust, high effective, and recycling magnetic sorbent for the removal of herbicides. J. Environ. Chem. Eng. 9, 104804.
Zavareh, S., Farrokhzad, Z., Darvishi, F.J.E., safety, e., 2018. Modification of zeolite 4A for use as an adsorbent for glyphosate and as an antibacterial agent for water. Ecotoxicol. Environ. Saf. 155, 1–8.
Zhang, X., Tang, D., Zhang, M., Yang, R.J.P.T., 2013. Synthesis of NaX zeolite: influence of crystallization time, temperature and batch molar ratio SiO2/Al2O3 on the particulate properties of zeolite crystals. Powder Technol. 235, 322–328.
Zhou, C.-F., Wang, Y.-J., Li, C.-C., Sun, R.-J., Yu, Y.-C., Zhou, D.-M.J.E.p., 2013. Subacute toxicity of copper and glyphosate and their interaction to earthworm (Eisenia fetida). Environ. Pollut. 180, 71–77.
Zhu, X., Li, B., Yang, J., Li, Y., Zhao, W., Shi, J., Gu, J., 2015. Effective adsorption and enhanced removal of organophosphorus pesticides from aqueous solution by Zr-based MOFs of UiO-67. ACS Appl. Mater. Interfaces 7, 223–231.